# NACA

### RESEARCH MEMORANDUM

EXPERIMENTAL RESULTS OF AN INVESTIGATION OF TWO METHODS

OF INFLIGHT THRUST MEASUREMENT APPLICABLE TO

AFTERBURNING TURBOJET ENGINES WITH EJECTORS

By Harry E. Bloomer

Lewis Flight Propulsion Laboratory Cleveland, Ohio

## NATIONAL ADVISORY COMMITTEE FOR AERONAUTICS

WASHINGTON

May 2, 1958 Declassified December 1, 1959

#### NATIONAL ADVISORY COMMITTEE FOR AERONAUTICS

#### RESEARCH MEMORANDUM

EXPERIMENTAL RESULTS OF AN INVESTIGATION OF TWO METHODS OF
INFLIGHT THRUST MEASUREMENT APPLICABLE TO AFTERBURNING
TURBOJET ENGINES WITH EJECTORS

By Harry E. Bloomer

#### SUMMARY

An investigation was conducted in an altitude test chamber using a turbojet engine equipped with an afterburner and ejector to compare directly two techniques of determining thrust that are both applicable to flight installations. One method is the use of a swinging uncooled rake at the ejector outlet. The other method requires extensive instrumentation to measure the momentum forces of the primary and secondary systems and the force on the internal surface of the ejector nozzle. The two methods are compared on the basis of accuracy, ease of installation, calibration required, and so forth. Comparisons are presented so that the reader can be guided to his own choice.

#### INTRODUCTION

During flight tests of prototype aircraft an accurate determination of the airframe drag is desired. In order to measure the drag in flight it is necessary to determine the actual propulsive force. Several experiments in thrust measurement have been conducted. The results of these tests are reported in references 1 to 6.

In view of the importance of flight thrust measurement, an investigation was made during part of the performance evaluation of a turbojet engine equipped with an afterburner and ejector to directly compare two techniques of determining thrust that are both applicable to flight installations. One method requires extensive instrumentation to measure accurately the internal momentum of the primary and secondary systems, the integrated static pressure on the internal surface of the ejector nozzle, and the geometry of the ejector. The second method requires only the integrated average of the total and static pressures at the ejector outlet with a swinging uncooled rake.

This report deals only with jet-thrust measurement. By applying other instrumentation to measure airflows as suggested in reference 3 and by knowing free-stream velocity, the net thrust and therefore airframe drag could be determined. Jet-thrust measurements alone are useful, however, for comparisons of prototype aircraft powerplants on a day-to-day basis during flight programs in which airframe configuration changes are made. They also permit comparison of the jet-thrust level with engine specifications.

The investigation was conducted in an NACA Lewis laboratory altitude test chamber. Thus, it was possible to measure actual thrust with the balance system to determine the accuracies of the two techniques. The engine is in the 10,000-pound-thrust class. The data cover a range of primary-pressure ratios from 2.0 to 10.35 and a range of secondary- to primary-flow ratios from 0.07 to 0.26 with the afterburner operating at a primary temperature of  $3400^{\circ}$  to  $3600^{\circ}$  R.

#### INSTALLATION AND INSTRUMENTATION

#### Installation

The ejector installation is shown schematically in figure 1. In this investigation the engine was operated at limiting exhaust gas temperature. Secondary air entered the test setup at an angle of  $90^{\circ}$  to the engine axis so that no extraneous axial force would be contributed. The entire assembly was mounted on a bedplate supported by flexure plates. Jet thrust was obtained from a calibrated null-type pneumatic cell after accounting for forces due to a pressure differential acting across the front-bulkhead labyrinth seal.

#### Instrumentation Applicable to Thrust Measurement

Internal-pressure technique. - The basic ejector instrumentation is shown in figure 2. Total pressures at stations s and p and total temperatures at s were computed as arithmetic averages since the probes were located in equal-flow areas. As a part of another investigation, the total-pressure drop from stations s to x was measured as a function of  $\rm p_{\rm s}/\rm P_{\rm s}$  (symbols are defined in appendix A). This pressure-drop curve is included in figure 13. Methods of calculation are given in appendix B. Ambient exhaust pressure was measured by four trailing static probes equally spaced around and 1 inch from the exhaust nozzle. Slide-wire potentiometers gave an indication of nozzle geometry.

NACA RM E57H28

Instrumentation used for measurement of thrust with this technique is itemized in the following table:

Quantity measured	Type of instrument	Number of instruments	Remarks
Primary total pressure, Pp	Total- pressure rake	2 to 4 rakes of 6 to 8 probes each	
Secondary total pressure, P <sub>s</sub>	Total- pressure probes	4 to 6 probes	
Wall static pressure, p <sub>w</sub>	Wall static- pressure orifices	Axial rows of 4 orifices spaced 2 to 4 in. apart	None required for cylindri- cal ejector
Ambient static pressure, p <sub>0</sub>	Trailing static- pressure probes	2 to 4 probes in plane of ejector nozzle l in. from lip	All tubes could be tied to one transducer
Primary- and secondary- nozzle geometry	Slide-wire potentiometers	One for each variable:  primary-nozzle di- ameter, secondary- nozzle diameter, and spacing ratio	None required for two- position noz- zle and fixed- shroud configuration

Since the facility pressure and temperature measuring systems were used for recording the steady-state data in this report, no transducers or recorders were needed. For a flight installation some remote means of recording these variables would be required.

Swinging-rake technique. - The swinging-rake details and actuating mechanism are shown in figure 3. The rake and hydraulic actuating mechanism were supplied by an airframe manufacturer. The rake was mounted independently of the engine in the test chamber so that the center probe passed through the geometric center of the nozzle. An instrumentation

summary including the type of transducers used for the swinging rake and their range is presented in the following table:

Pressure measured	Type of transducer	Pickup size, lb/sq in.	Manufacturer
Total	Strain-gage	<u>+</u> 50	Statham No. 131
Static	Strain-gage	<u>+</u> 10	Control Engineering Corp. C.E.C. No. 4-312

The angular position of the rake was sensed with a slide wire with built-in reference markers indicating up to 75° of rotation. Using solenoid valves and a vacuum pump, the transducers were calibrated by venting the reference side to the low-pressure source and by assuming that the pressure side was equal to test-chamber static pressure. This was done with the test chamber open and with the engine on full after-burning at an altitude flight condition. The transducers and slide wire were located in air-cooled boxes. The outputs from the transducers and slide wire reference pressure for the transducers was test-chamber static pressure. For a flight installation, of course, this would be a different pressure.

Instrumentation used for measurement of thrust with the swinging rake is itemized in the following table:

Quantity measured	Type of Instrument	Number of Instruments	Remarks
Rake total pressure, Pr	Probe on rake	l to 3 probes on rake	
Rake static pressure, p <sub>r</sub>	Static-pressure orifices on probe body	l to 3 probes on rake with 4 to 6 ori- fices per probe	
Reference pressure, pref	Static-pressure orifice	1	Could be same as ambient pressure
Ambient static pressure, p <sub>0</sub>	Trailing static- pressure probes	2 to 4 probes in plane of ejector nozzle l in. from tip	All tubes could be tied to one transducer
Rake position	Slide-wire potentiometer	1	

NACA RM E57H28

The hydraulic actuator used to swing the rake operated on a pressure of 1500 pounds per square inch and was supplied with restrictions that allowed the rake to make a required traverse of the nozzle in 6 seconds or less. The rake was made of stainless steel and was not cooled because the traverse was rapid enough to prevent overheating. It was positioned outside the exhaust jet, except when traversing, to keep it cool.

#### PROCEDURE

During the ejector evaluation when several engine-inlet flight conditions were being simulated, the primary-pressure ratio was varied from 2.0 to about 10.5. The secondary-weight-flow ratio was also varied from 0.07 to 0.27. While a steady-state data point was being obtained for use with the internal-pressure technique, the rake was swung through the jet from right to left. Then, after approximately 20 seconds of cooling time, the rake was returned across the jet to its original position. The data from each traverse were reduced in the following manner: The oscillograph traces of the swings were processed by reading the deflection of the pressure and position traces at selected time intervals with a telereader machine. These readings were punched on IBM cards and fed into an IBM 650 magnetic-drum data-processing machine along with a program to achieve a point-to-point integration of the thrust against area curve.

The data for the internal-pressure method were processed by taking the pressures, temperatures, and so forth, and calculating the thrust manually. For a long program, however, this could be done through a data-processing machine.

#### RESULTS

#### Swinging-Rake Technique

Assumptions for swinging-rake technique. - Assumptions made for the swinging-rake technique were as follows: Since the static pressure is measured in a plane 3.5 inches downstream of the total pressure, it was assumed that the static-pressure measurement was valid and could be used to correct the total pressure in the plane 3.5 inches upstream. The time-lag constants of the pressure systems were assumed to be negligible. It was assumed that for the circular exit of this tailpipe the conditions around any radius would be equal; thus, the conditions measured across one diameter could be applied to the exit area. It also was assumed that the ratio of specific heats  $\gamma$  was constant for the entire swing.

Effects of yaw angle. - The effect of yaw angle on the variation of the pressure-correction ratio with indicated-pressure ratio is presented in figure 4. The data points were obtained during the installation of the swinging rake in the NACA Lewis laboratory 8- by 6-foot supersonic wind tunnel. The extrapolations of the data curves and the addition of the curves for  $15^{\circ}$ ,  $17\frac{1}{2}^{\circ}$ , and  $20^{\circ}$  angles of yaw in figure 4(a) were guided by calibration data obtained in references 7 and 8.

From figure 4(b) and reference 9, it was assumed that  $20^{\circ}$  of yaw would not affect the total-pressure calibration.

Typical oscillograph trace. - A typical oscillograph record of the position and pressure traces is presented in figure 5 for the swing in one direction. It should be noted that the places where the deflections were read were strategically placed in order to obtain a good point-to-point integration. The position trace is nearly linear with time.

Indicated-pressure profiles. - The variation of the indicated pressures with radius from the record of figure 5 is presented in figure 6. Note that the radius is given from the nozzle centerline. Hence, the top and bottom probes never reach radii less than the fixed minimum values. The variation in the indicated pressures for the top and bottom probes on the left side of the jet should be noted. This probably is due to some asymmetry in the nozzle geometry or secondary-flow distribution around the ejector. It is also possible that the rake body actually was deflected along its axis because of a combination of aerodynamic disturbances and thermal stresses as it entered the 3600° R high-velocity jet.

The effect of primary-nozzle pressure ratio on the variation of indicated pressure with radius for the center probe only is presented in figure 7. Swings in both directions show good reproducibility except for the left side of the jet boundary. The profile of the low-pressure-ratio case (fig. 7(a)) shows a marked asymmetry compared with the higher pressure-ratio profiles. Any slight nonconcentricity of the nozzle could cause this at these low-pressure ratios.

Sources of error in thrust measurement with swinging rake. - The final thrust answer depends on which static-pressure calibration curve is used. Since the static pressure is used to correct the total pressure for bow shock, it would seem that large thrust errors might accrue. Figure 8 is presented to show the effect of percent error in static-pressure measurement on the variation of percent error in gross thrust per unit area with true jet-exit pressure ratio. From this figure, it can be seen that, at a pressure ratio of 10, a  $\pm 30$ -percent error in static-pressure measurement can make only a  $\pm 2.2$ -percent error in gross thrust.

NACA RM E57H28

This effect of static-pressure change on thrust can also be shown for experimental data. Using each of the static-pressure calibration curves (fig. 4(a)), the gross-thrust values were calculated for each point read on the oscillograph traces and were integrated point by point over the area. (The methods used are reported in appendix B.) The gross-thrust answers were divided into the reference thrust to form a thrust-correlation factor, and the results for the one swing shown in figure 5 are presented in figure 9. It can be noted from this figure that using no calibration curve for static pressure results in about a 5-percent error. As the yaw-angle correction for static pressure increases to 20° the thrust error decreases to 2 percent. The question of which yaw-angle correction curve should be used was solved by comparing the corrected total-pressure profiles with the primary-pipe total pressure as measured by the water-cooled rake.

Corrected-pressure profiles. - The corrected-pressure profiles for the swing shown in figure 5 are presented in figure 10 for each static-pressure yaw-angle calibration.

It should be noted that the peaks and valleys in total pressure reflect the opposite trend in static pressure. As the yaw-angle correction becomes greater, the peaks and valleys level out and produce a believable average total pressure as compared with the water-cooled-rake total pressure in the primary pipe. This occurs at  $17\frac{1}{2}^{\circ}$ -yaw-angle correction. The primary total pressure is shown in figure 10(e) for reference. The peaks and valleys still occur in this figure but they can be explained by the fact that the plane of the static-pressure orifices is 3.5 inches downstream of the plane of the total-pressure orifices. Any formation of compression and expansion waves in the jet between the two stations can cause the wrong static pressure to be used to correct the total pressure for bow shock. The true corrected total pressure should be similar in shape to the indicated total-pressure profiles presented in figures 6 and 7. Therefore, the  $17\frac{1}{2}^{\circ}$ -yaw-angle correction was used for the processing of the data.

It is realized that probably no primary-total-pressure instrumentation would be available in a flight installation to check the correct total-pressure level. From previous experience, flow yaw angles of 10° to 20° should be expected and necessary calibration corrections should be applied.

Thrust-correlation factors. - The variation of thrust-correlation factor with primary-nozzle pressure ratio for all the swings recorded is presented in figure 11. Since all but two of the left-to-right points fell above the right-to-left points, it was suspected that there was some hysteresis in the position indication. With reference to the oscillograph traces, it could be seen that most of the left-to-right records

showed some position-indication discontinuity as the rake entered the jet. The small position-trace discontinuity shown in figure 5 caused the thrust-correlation factor to increase 2 percent (tailed symbol in fig. 11), from the right-to-left swing. The greatest discrepancy in thrust between swings was 8 percent. The smallest discrepancy is about 1/2percent where no trace discontinuity was noticed. This position-trace discontinuity was not present for any of the right-to-left traces. The asymmetric profile presented in figure 7(a) probably causes the thrustcorrelation factor to deviate at the low primary-nozzle pressure ratio. It is quite likely that variations in pressure occur circumferentially that are not accounted for by the rake swinging in one path. Since no present airplane-engine configuration would fly at this nozzle pressure ratio, only preflight check data would be affected. Therefore, neglecting the left-to-right swings and the low pressure ratio, figure 10(b) indicates that thrust could be predicted with an accuracy of  $\pm l\frac{1}{2}$  percent, if the proper yaw correction can be applied to the data.

#### Internal-Pressure Technique

Assumptions. - For this ejector and for all high-performance airplane ejector configurations (where the boattail angles and, hence, the ejector included angle deviate little from the axial centerline), assumptions can be made to eliminate much of the instrumentation formerly needed to calculate basic primary and secondary flows.

The first assumption is that the arithmetic average of the pressures measured along the internal surface of the ejector nozzle equals the integrated average of the pressures along the surface.

The second assumption that can be applied is that

$$F_p = A_{p,x}(1.25P_p - p_0)$$

for the afterburning case. (Use 1.265 for nonafterburning, ref. 7.)

The third assumption is that

$$A_{s,x}(P_x - p_0) \cong \frac{w_s^2 t_x}{p_x A_{s,x}} \frac{R}{g} + A_{s,x}(p_x - p_0)$$

An examination of the calculated data shows that this is a reasonable assumption. For the ejector investigated, where the secondary-nozzle included angle was not more than 12° when convergent or 6° when divergent, the inequality in the equation was less than 3 percent for low weight-flow ratios and less than 10 percent for high weight flows. In these cases, the resultant error to the gross thrust would be less than

 $\frac{1}{2}$  percent.

By applying these assumptions, it would be necessary to measure only primary and secondary total pressure, ambient pressure, ejector internal static pressure, and ejector geometry.

Thrust-correlation factors. - The results of this method of measuring thrust are presented in figure 12 as the variation of thrust-correlation factor with primary-nozzle pressure ratio. The circular symbols indicate data taken coincidentally with the rake swings. Other data are presented to show that there is no effect of ejector geometry on the correlation. The maximum deviation of the data points from the curve is about 1.5 percent. The increase in thrust-correlation factor from 0.95 to 1.0 with pressure ratio could be due to increased leakage in the primary-nozzle segments at high pressure ratio.

#### SUMMARY OF RESULTS

The two methods of thrust measurement are compared in the following table on the basis of accuracy, ease of installation, calibration required, and so forth. Comparisons are presented so that the reader can be guided to his own choice.

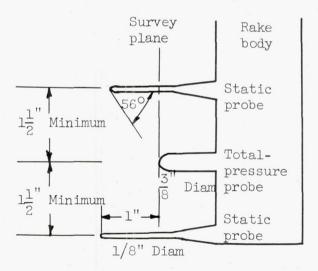
Basis of Comparison	Internal-pressure method	Swinging-rake method
Over-all accuracy using correlation curves	$\pm l\frac{1}{2}$ percent	$\pm l\frac{1}{2}$ percent
Over-all accuracy without using correlation curves	5 percent	5 percent
Parameters that most affect thrust answer	Primary total pressure and primary- nozzle area	Rake position
Total number of instrumentation channels, minimum and maximum	20 and 58	4 and 9
Complication of installation (biggest problem)	Cooled rake for measuring primary total pressure	Installing actuator mechanism so that position geometry will be correct
Calibration for pressure instru- mentation required (yaw and supersonic flow corrections)	No	Yes
Number of position calibrations required	3: Primary-nozzle diameter, secondary- nozzle diameter, spacing ratio	1: Rake position
Number of record points to be read for each data point	l for each channel of instrumentation	40 to 60 for each channel of instrumentation
Instrumentation effect on air- frame external drag	None	Amount depends on cleanness of installation of actuator and rake
Instrumentation effect on engine thrust	Very little; both primary and secondary streams are low subsonic velocity at instrumentation stations	Drag on rake body is estimated equal to about 2 percent of engine thrust

The difficulty in obtaining the respective correlation curves might well influence the choice between the two systems. Obviously a full-scale engine-ejector calibration to determine a curve similar to figure 12 would be more difficult to obtain than the yaw-angle calibration of a probe such as figure 4.

#### POSSIBILITIES FOR IMPROVEMENT OF METHODS

A more reliable position indicator should be incorporated on the swinging rake. Possibly an angle sensor should be added to the rake instead of one of the Pitot tubes so that proper angle corrections could be made to the static-pressure measurement during the swing.

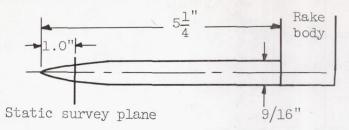
Another method of improvement to the accuracy of static-pressure measurement in the swinging rake would be to put the orifices at least 8 tube diameters back of the leading edge of the probe (ref. 4). This, of course, has the disadvantage of making the axial distance larger between the measuring stations of the total and static pressures. The diameter of the probe could be made smaller to obviate this. However, the pressures could be measured in the same axial plane by separating the probes as in the following sketch:



At each point during the swing, the static pressures could be averaged since the static-pressure gradient is not steep and the probes would be at approximately the same radius from the nozzle center. As a matter of simplification, the pressure leads from the static-pressure probes could be tied to the same transducer and the approximate average static pressure would result.

NACA RM E57H28

Another possibility would be to make an ogive-shaped probe. A quarter-scale model from reference 10 is sketched below:



Then, knowing the pressure distribution about an ogive-shaped body at supersonic speeds from reference 10, a correction for the effect of axial deviation could be made to the static-pressure measurement.

Another possibility would be to incorporate a sonic aspirated thermocouple and total-pressure probe on the rake. Rolls and Havill use one such type (ref. 2). However, the probe reported in reference 11 is also another possibility.

Lewis Flight Propulsion Laboratory
National Advisory Committee for Aeronautics
Cleveland, Ohio, September 20, 1957

#### APPENDIX A

#### SYMBOLS

A	area, sq ft	
С	chord length, in.	
D	diameter	
F	jet thrust, lb	
g	acceleration due to gravity, 32.17 ft/sec <sup>2</sup>	
L	spacing, axial distance between primary- and secondary-nozzle exits, in.	
1	radius of swing, in.	
M	Mach number	
P	total pressure, lb/sq ft abs	
р	static pressure, lb/sq ft abs	
R	universal gas constant	
t	static temperature	
W	measured weight flow, lb/sec	
Υ	ratio of specific heats for afterburning gas stream, 1.27	
θ	angular deflection of swinging rake from center of traverse	
Subscripts:		
a,b,c,d	internal stations	
calc	calculated	
corr	corrected	

primary

p

indicated swinging-rake measurement ref reference secondary wall plane of primary-nozzle exit

o ambient, or plane of secondary-nozzle exit

Superscript:

averaged

#### APPENDIX B

#### METHODS OF CALCULATION

#### Swinging-Rake Pressure Corrections

The procedure for correcting swinging-rake indicated pressures is as follows:

- (1) Form the indicated pressure ratio  $p_r/P_r$
- (2) Read static-pressure correction ratio  $p_r/p_{r,corr}$  from calibration curve like figure 4(a)
  - (3) Correct static pressure:  $p_{r,corr} = \frac{p_r}{p_r/p_{r,corr}}$
- (4) Since there is no yaw correction for total pressure (fig. 4(b)) form the new pressure ratio  $p_{r,corr}/P_r$ , and find  $P_r/P_{r,corr}$  from the following relationships:

$$P_{r}/P_{r,corr} = \left[\frac{(\gamma + 1)M^{2}}{(\gamma - 1)M^{2} + 2}\right]^{\frac{\gamma}{\gamma - 1}} \left[\frac{\gamma + 1}{2\gamma M^{2} - (\gamma - 1)}\right]^{\frac{1}{\gamma - 1}}$$

where M is determined from

$$P_{r}/p_{r,corr} = \left[\frac{(\gamma + 1)M^{2}}{2}\right]^{\frac{\gamma}{\gamma - 1}} \left[\frac{\gamma + 1}{2\gamma M^{2} - (\gamma - 1)}\right]^{\frac{1}{\gamma - 1}}$$
 (Rayleigh Pitot formula)

and  $\gamma$  is assumed 1.27 for afterburning case.

(5) Then correct total pressure 
$$P_{r,corr} = \frac{P_r}{P_r/P_{r,corr}}$$

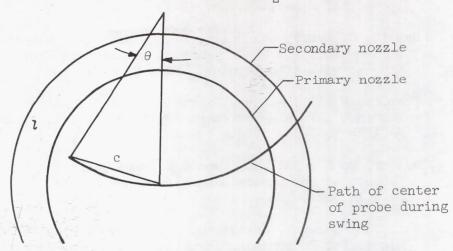
Thrust Calculation for Swinging-Rake Technique

Thrust at each point along the traverse is then calculated from the following:

$$\frac{F_r}{A_r} = p_r \left[ \frac{2\gamma}{\gamma - 1} \left( \frac{P_r}{p_r} \right)^{\frac{\gamma - 1}{\gamma}} - \frac{\gamma + 1}{\gamma - 1} \right] - p_0$$

Area is determined from the radius of the probe from the center of the nozzle. Radius is determined from the swinging-rake geometry and the following equation:

Chord length = radius =  $27 \sin \frac{1}{2} \theta$ 



Gross thrust is then determined by a point-to-point integration of the parameter F/A against area of the entire swing.

Thrust Calculation for Internal-Pressure Technique

The thrust for the internal-pressure technique is determined from the following equation:

$$F_{\text{calc}} = F_{p} + \frac{w_{s}^{2}t_{x}}{p_{x}A_{s,x}} \frac{R}{g} + A_{s,x}(p_{x} - p_{0}) + A_{0}p_{0} - \int_{0}^{x} (\overline{p_{a} + p_{b} + p_{c} + p_{d}}) dA_{0}$$

The explanation for the further simplification of this equation is contained in the Assumptions section of the RESULTS. The simplified equation is

$$F_{\text{calc}} \cong A_{p,x}(1.25P_p - p_0) + A_{s,x}(P_x - p_0) - A_0 \left[ (p_a + p_b + p_c + p_d) - p_0 \right]$$

The values of  $P_{\mathbf{x}}$  were obtained from the pressure-drop curve shown in figure 13 of this report.

#### REFERENCES

- 1. Rolls, L. Stewart, and Havill, D. Dewey: Method for Measuring Thrust in Flight on Afterburner-Equipped Airplanes. Aero. Eng. Rev., vol. 13, no. 1, Jan. 1954, pp. 45-49.
- 2. Havill, C. Dewey, and Rolls, L. Stewart: A Sonic-Flow Orifice Probe for the Inflight Measurement of Temperature Profiles of a Jet Engine Exhaust with Afterburning. NACA TN 3714, 1956.
- 3. Fleming, William A., and Gabriel, David S.: A Survey of Methods for Turbojet Thrust Measurement Applicable to Flight Installations. NACA RM E55DO5a, 1955.
- 4. Beller, De E., Bellman, Donald R., and Saltzman, Edwin J.: Flight Techniques for Determining Airplane Drag at High Mach Numbers. NACA TN 3821, 1956.
- 5. Rolls, L. Stewart, Havill, C. Dewey, and Holden, George R.: Techniques for Determining Thrust in Flight for Airplanes Equipped with Afterburners. NACA RM A52Kl2, 1953.
- 6. Sivo, Joseph N., and Fenn, David B.: A Method of Measuring Jet Thrust of Turbojet Engines in Flight Installations. NACA RM E53J15, 1954.
- 7. Hasel, Lowell E., and Coletti, Donald E.: Investigation of Two Pitot-Static Tubes at Supersonic Speeds. NACA RM L8102, 1948.
- 8. Gracey, William, and Scheithauer, Elwood F.: Flight Investigation at Large Angles of Attack of the Static-Pressure Errors of a Service Pitot-Static Tube Having a Modified Orifice Configuration. NACA TN 3159, 1954.
- 9. Gracey, William: Wind-Tunnel Investigation of a Number of Total-Pressure Tubes at High Angles of Attack. Subsonic, Transonic, and Supersonic Speeds. NACA TN 3641, 1956.
- 10. Jack, John R., and Burgess, Warren C.: Aerodynamics of Slender Bodies at Mach Number of 3.12 and Reynolds Numbers from 2×10<sup>6</sup> to 15×10<sup>6</sup>. I Body of Revolution with Near-Parabolic Forebody and Cylindrical Afterbody. NACA RM E51H13, 1951.
- ll. Glawe, George E.: A High Temperature Combination Sonic Aspirated Thermocouple and Total Pressure Probe. Jet Prop., vol. 27, no. 5, May 1957, pp. 543-544.

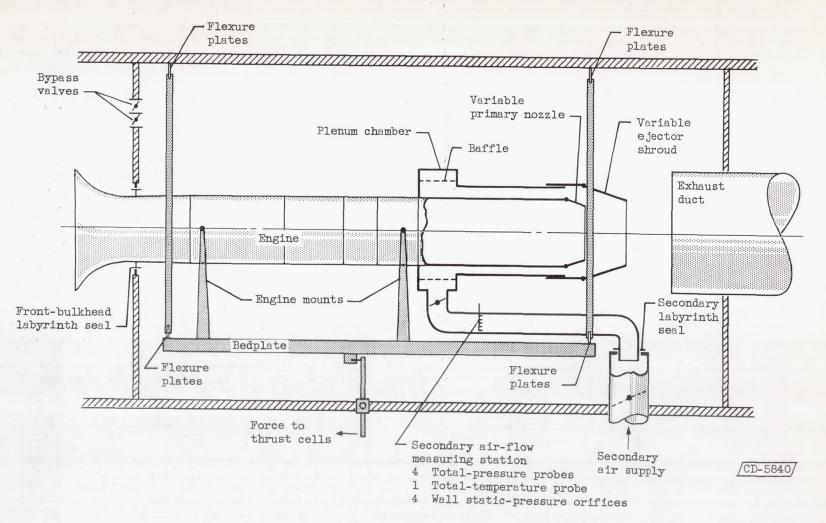


Figure 1. - Schematic drawing of test installation.

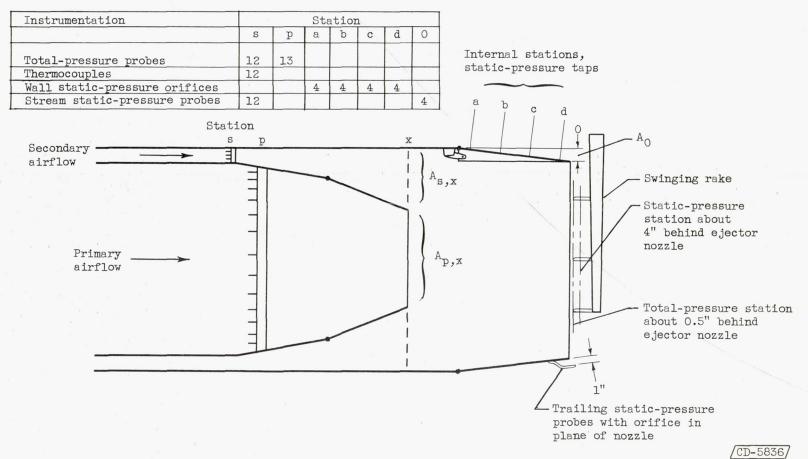
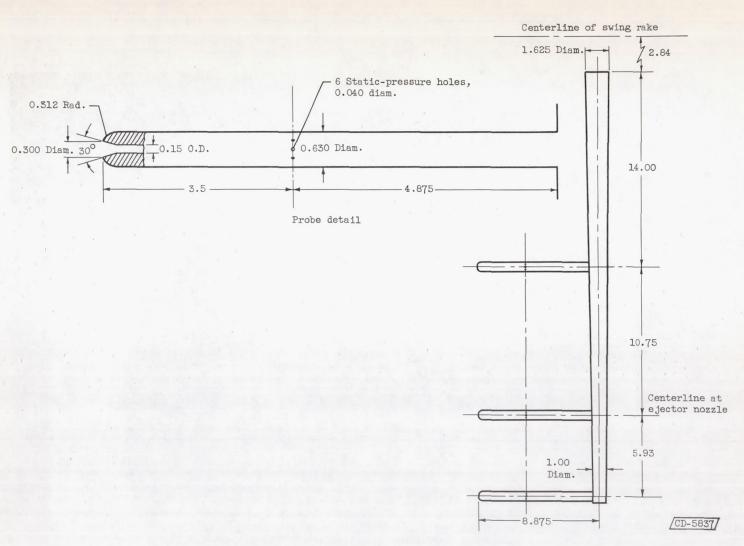
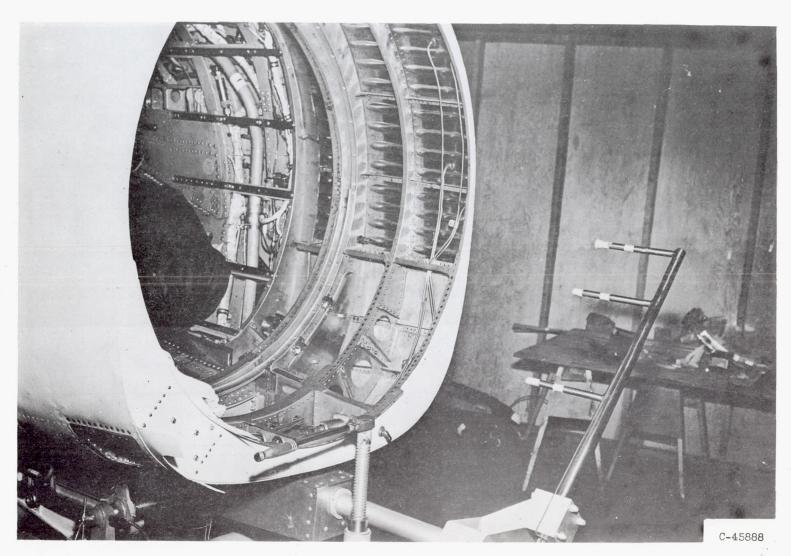


Figure 2. - Schematic drawing showing instrumentation stations and ejector installation.



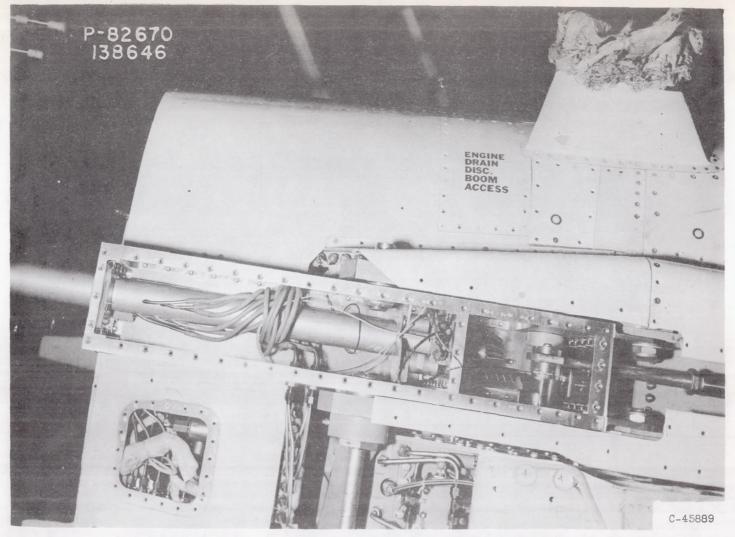
(a) Detail of probe showing general dimensions in inches.

Figure 3. - Swinging rake used in investigation.



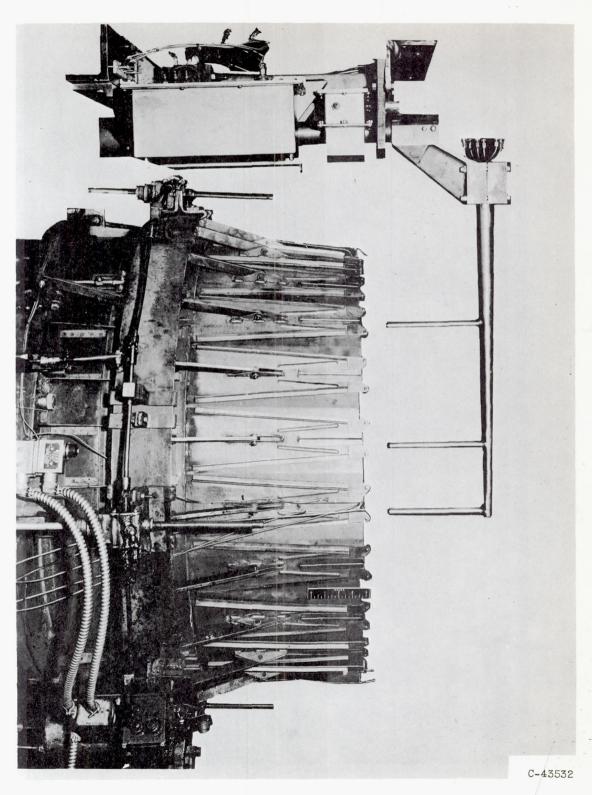
(b) Rake mounted on airframe. (Grumman Aircraft Eng. Corp. photograph.)

Figure 3. - Continued. Swinging rake used in investigation.



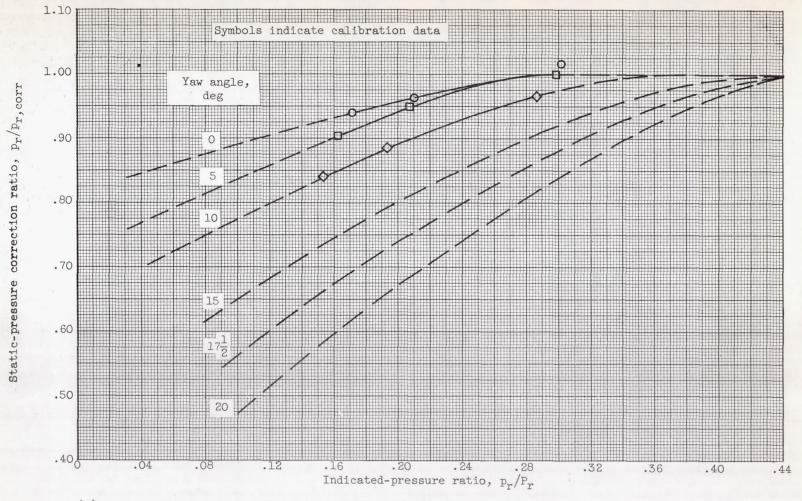
(c) Details of rake actuating mechanism mounted on airframe. (Grumman Aircraft Eng. Corp. photograph.)

Figure 3. - Continued. Swinging rake used in investigation.



(d) Relative positions of rake and variable ejector used during investigation.

Figure 3. - Concluded. Swinging rake used in investigation.



(a) Static-pressure correction ratio; static-pressure orifice 5.5 diameters behind probe nose and 7.75 diameters ahead of rake body.

Figure 4. - Variation of pressure-correction ratio with indicated-pressure ratio showing effect of yaw angle of flow.

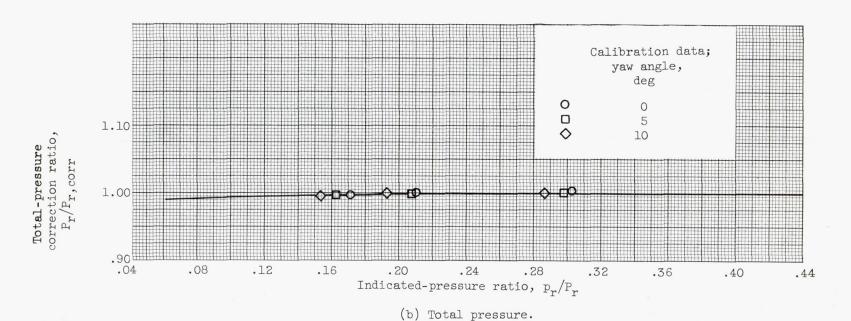


Figure 4. - Concluded. Variation of pressure-correction ratio with indicated-pressure ratio showing effect of yaw angle of flow.

4546

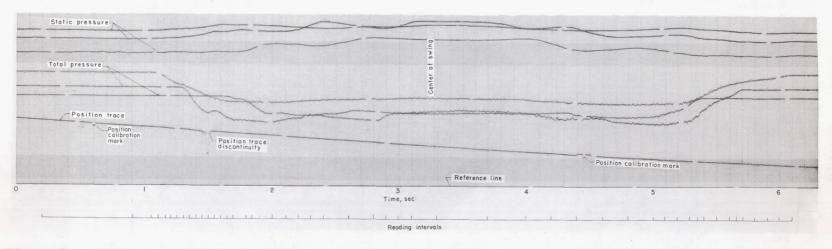


Figure 5. - Typical oscillograph record of pressures and position traces during rake swing in one direction.

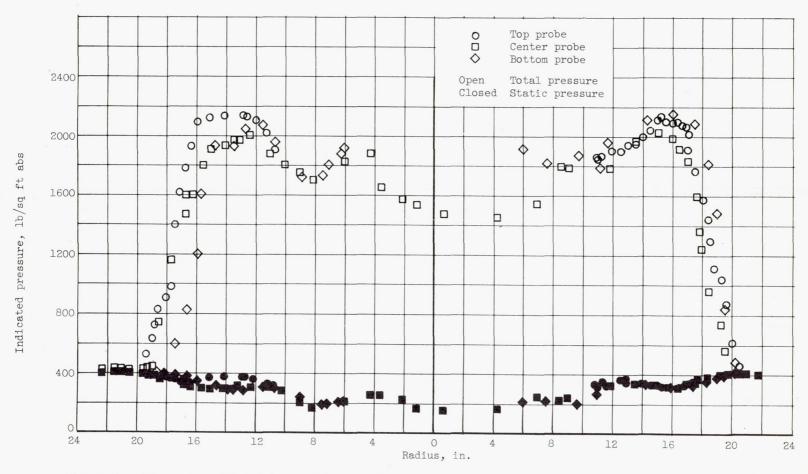


Figure 6. - Pressure profiles determined by swinging rake showing comparisons of three probes. Engine-inlet simulated flight conditions, altitude of 35,000 feet at Mach number of 1.16; secondary-flow ratio, 0.136; primary-nozzle pressure ratio, 6.01.

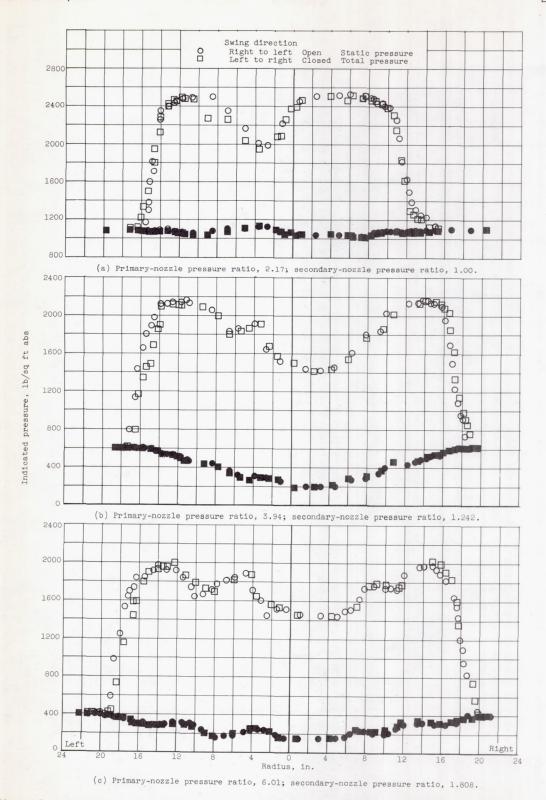
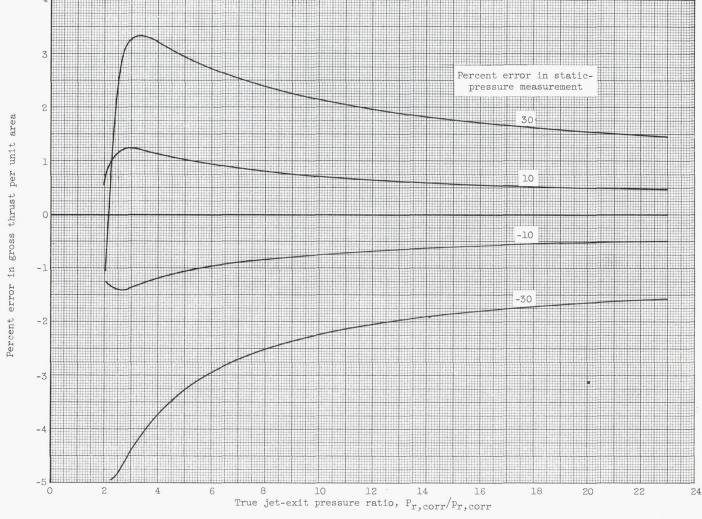


Figure 7. - Variation of indicated pressure with radius during rake swing. Engine-inlet simulated flight conditions, altitude, 35,000 feet and Mach number of 1.16; secondary air weight-flow ratio, 0.136.



CONFIDENTIAL

Figure 8. - Effect of static-pressure measurement error on variation of percent error in gross thrust per unit area with true jet-exit pressure ratio. Curves assume that ambient pressure equals true rake static pressure. Procedure for thrust-per-area calculation is given in appendix B.

CONFIDENTIAL

CONFIDENTIAL

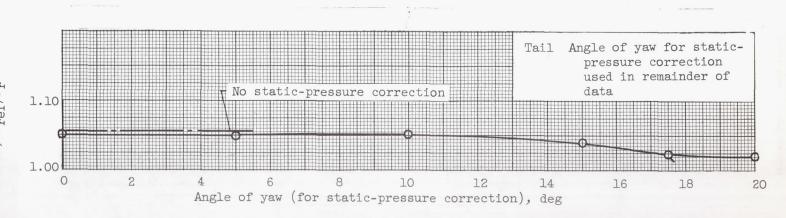


Figure 9. - Variation of thrust-correlation factor with static-pressure correction.

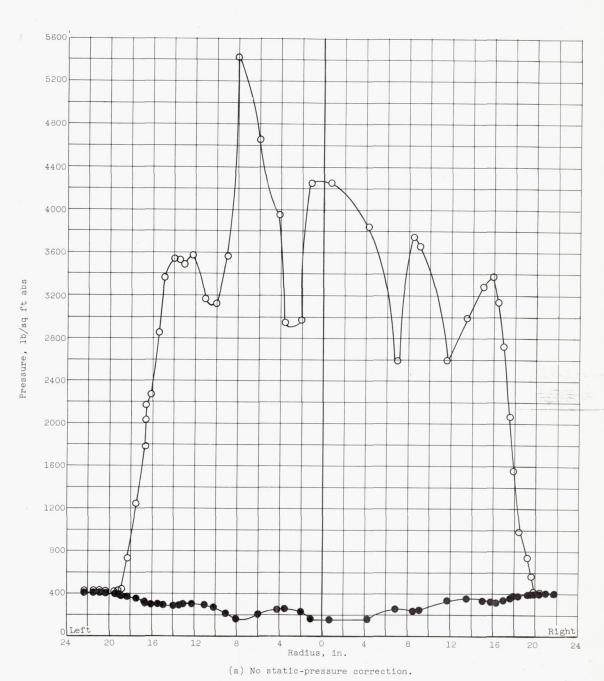
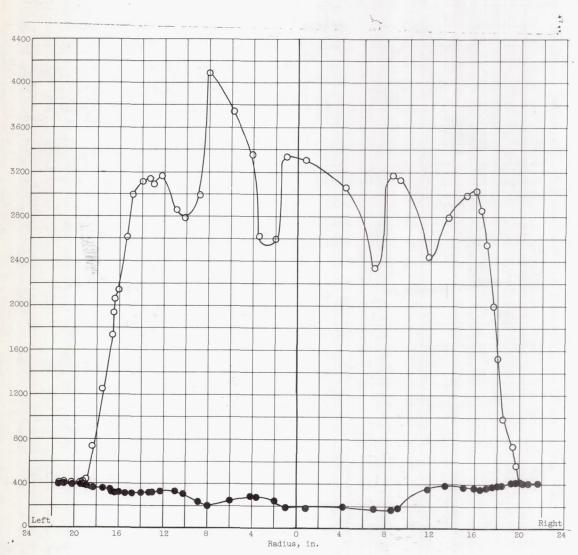


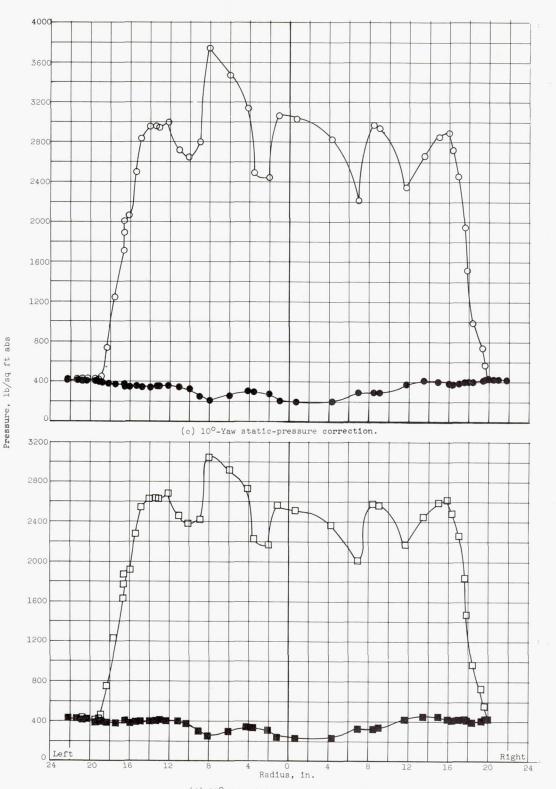
Figure 10. - Effect of various static-pressure corrections on the variation of calculated pressure with radius.



(b) 5°-Yaw static-pressure correction.

Figure 10. - Continued. Effect of various static-pressure corrections on the variation of calculated pressure with radius.





(d)  $15^{\circ}$ -Yaw static-pressure correction.

Figure 10. - Continued. Effect of various static-pressure corrections on the variation of calculated pressure with radius.

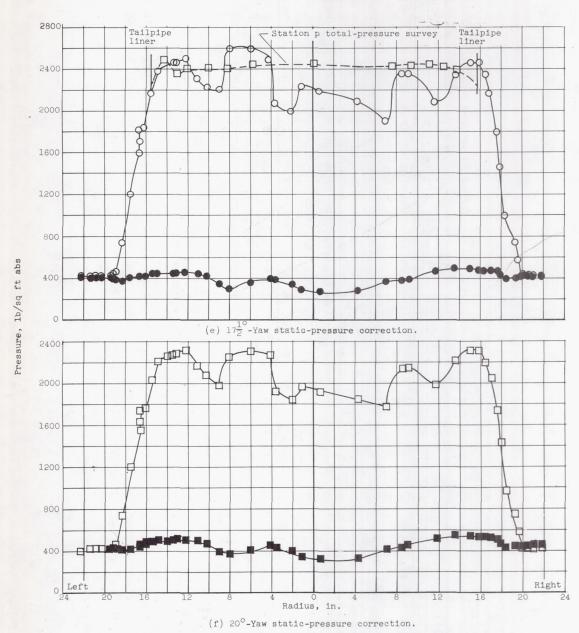


Figure 10. - Concluded. Effect of various static-pressure corrections on the variation of calculated pressure with radius.

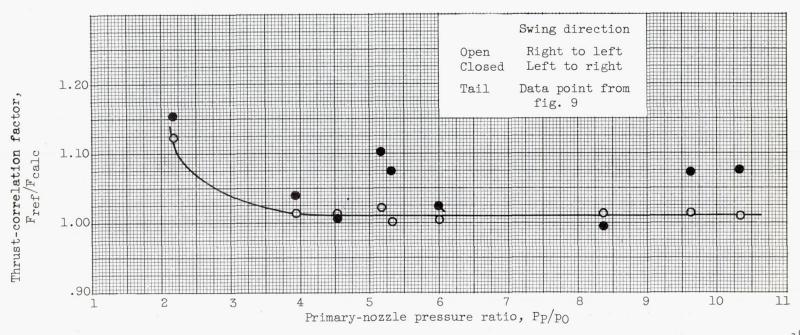


Figure 11. - Variation of thrust-correlation factor with primary-nozzle pressure ratio using  $17\frac{1}{2}$  - yaw static-pressure correction curve. Secondary-flow ratio varies from 0.07 to 0.24; diameter ratio of ejector is approximately 1.25.

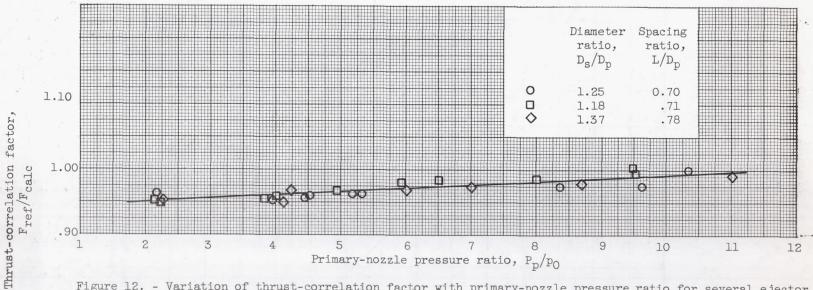


Figure 12. - Variation of thrust-correlation factor with primary-nozzle pressure ratio for several ejector configurations. Secondary-flow ratio varies from 0.03 to 0.28.

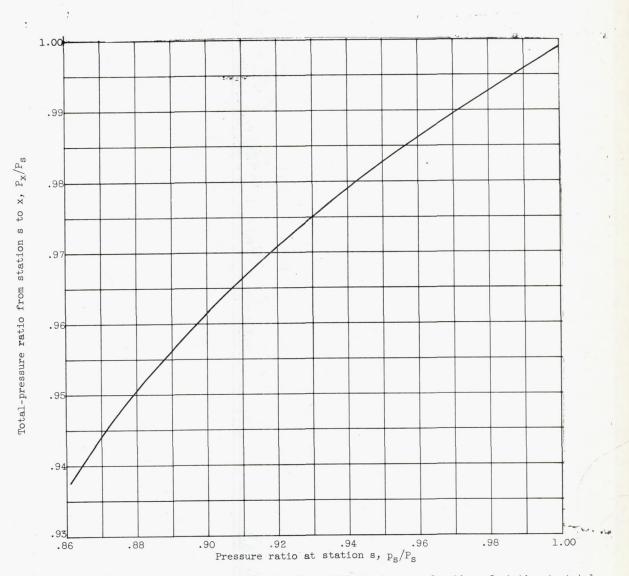


Figure 13. - Total-pressure-loss ratio from station s to x as function of static- to total-pressure ratio at station s.